The Zeeman Effect

Splitting emission spectra with an electromagnet to find the magnetic moment of the electron

March 14, 2020

Report by Xavier Boluna in collaboration
with Ryota Johnson & Sahar Ahmadi

ABSTRACT

This report recreates the Zeeman experiment, performed first by Pieter Zeeman in 1887. The experiment, which won a Nobel Prize with the contribitions of Hendrik Lorentz, relates the splitting of emission spectra by a powerful electromagnet with the quantum properties of the electron. This experiment was performed at the incipience of the discovery of the atomic structure and was revolutionary in its derivation of the Bohr magneton μ_0, which encapsulates the quantum numbers of angular and orbital momenta of the electron in relationship to its emission of light.

This report, in multiple steps, derives the Bohr magneton using two different polarizations for light in the area of 546 nm. Using an electromagnet and a Fabry-Perot interferometer, emission spectra are created and split under the conditions of the Zeeman effect and related to the universal constant of the Bohr magneton.

The 0 and 90° polarizations (known as π and σ polarization) filter out different transmissions of light and allow for two different techniques to calculate the magneton. For each polarization, we calculated values of $\mu_0 = (9.662 \pm 0.135) \times 10^{-24}$ J/T and $\mu_0 = (8.673 \pm 0.369) \times 10^{-24}$ J/T, respectively. This is in significant agreement with the reference value provided by the NIST (see Appendix), with one-tailed p-values of 13 and 25.4%, respectively.

A schematic of the optical rail used to investigate the Zeeman effect and derive the Bohr magneton.

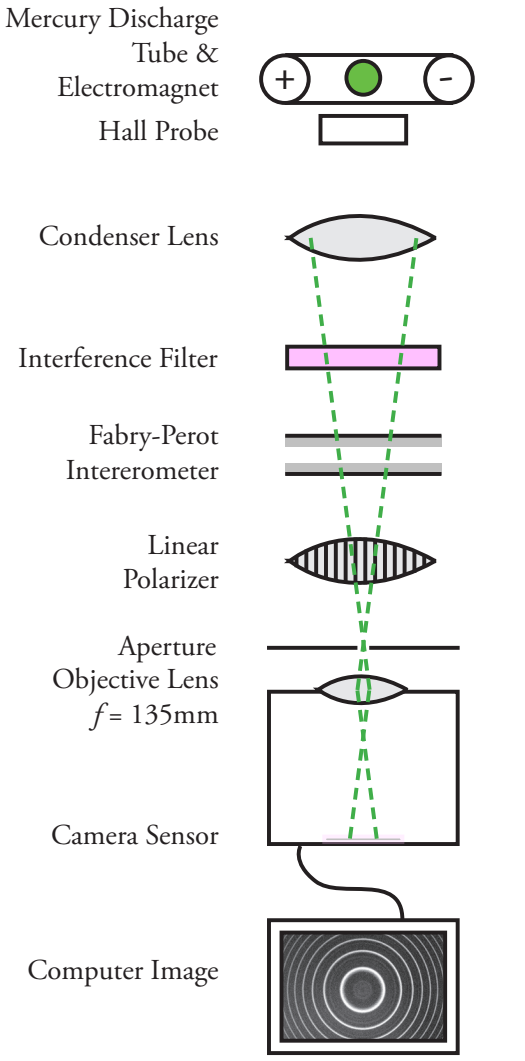

Introduction

In 1902, Pieter Zeeman won the Nobel Prize for research conducted alongside Hendrik Lorentz. The research that won them the prize involved a simple idea: measure the effect of magnetism on light. The results, however, wholly transformed the contemporary understanding of light emission and laid groundwork for the discovery of the electron.

In 1886, however, Zeeman's goals were quite a bit simpler. *Over de invloed eener magnetisatie op den aard van het door een stof uitgezonden licht*, his paper on the 'effect of magnetism on a light-emitting substance,' describes his intuitions on the subject (Zeeman, 1887). In Maxwell's *Collected Works vol. 2*, he describes testing the effects of a powerful magnet on a flame to no apparent results. Zeeman reasoned that the application of modern (and much higher-resolution) spectroscopy could produce different results.

Zeeman witnessed a phenomena which required the efforts of another, more experienced physicist to describe -- at least mathematically. Lorentz was in the process of developing theories on electromagnetic radiation, including minute oscillating particles which he described as negatively charged and responsible for the emission of light. Thomson would describe these oscillating particles in 1904 as negatively-charged 'corpuscles,' surrounding a sphere of positive charge. Later, physicists, would prefer the term 'electron.'

This is all to say that Zeeman's experiment proved crucial in building the evidence to support theories for electrons, electron spin and quantum particles. While Zeeman's experiment purely concerned the effects of a magnet on the spectral lines of Sodium, modern understanding explains in greater detail the quantum interactions between paired electrons.

Take the example of Mercury. Subject to electrical discharge, just one of its 6s electrons is excited to a higher state, 7s. As the electron de-excitates, it releases two successive photons (packets of light) until it reaches its original equilibrium state:

$$(6s)\cdot(6s) \rightarrow (6s)\cdot(7s) \dashrightarrow (6s)\cdot(6p) \rightarrow (6s)\cdot(6s)$$

transition in 10^{-9} seconds

$^1S_0$ $^3S_1$ $^1P_1$ $^3P_0$ $^3P_1$ $^3P_2$

λ = 546.07 nm

The transition we are interested occurs in one millionth of a second and, in some cases, as $^3S_1 \rightarrow {}^3P_2$. When this single case of 8 occurs, a bright burst of green light is emitted at a wavelength of 546.07 nanometers.

As Figure One illustrates, we can pass this light through an interference filter to eliminate the light from other emissions in the visual spectrum. From here, we can use a spectrometer to create interference lines.

The Fabry-Perot interferometer is a high-resolution spectroscope which takes advantage of a millmetric gap between two highly reflective panels to produce interference fringes of increasing order. Each of these individual fringes, as shown in Figure Two (a), has an associated angle θ with respect to the optical axis (Brown, 2019).

As these rays travel over a horizontal distance parallel to the optical axis, their vertical position increases as a function of their angle. We use a camera to capture an image of the interference pattern, with a fixed resolution. In our case, with a focal length of 135 millimeters, every pixel corresponds to a 9×9 micrometer square. Figure Two (b) is an image of these lines where, as a result of the radial symmetry of the incident and transmitted light, a ringed interference pattern occurs.

The geometries associated with the Fabry-Perot are described in greater detail in (Brown, 2019), however we briefly mention that the slope of the squared angle equals the emission wavelength divided by the mirror separation, 6.499 mm, such that $\frac{d\theta^2}{dt} = \frac{\lambda}{t}$.

The introduction of a magnetic field drastically changes the situation. The comprehensive explanation of the Zeeman effect involves quantum mechanical properties of spin S, orbital (angular) momentum L and

Pieter Zeeman's photograph of the splitting of interference lines under the effect of magnetism

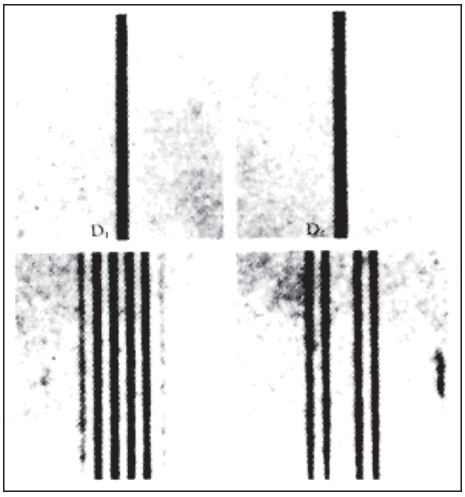

Under no magnetic influence (B = 0)

Under a non-zero magnetic influence (B > 0)

Zeeman's exploration of emission splitting used a Sodium lamp and a Fabry-Perot interferometer. The upper lines are the the D-lines of Sodium which are then split by a magnetic field, resulting in the multiple lines seen in the bottom half of the image.

Figure One: Optical Interference Filter

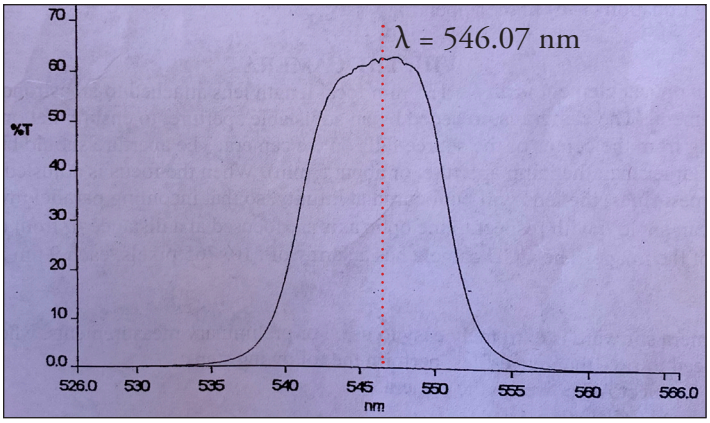

The purpose of the interference filter is to allow light in a narrow band of wavelengths to pass, while other light is occluded. This filter allows a percentage of light transmission (%T) up to about 63% around 547 nanometers. Our target wavelength is 546.07 nm.

The transmission dies off quickly, with less than 10% transmission for wavelengths outside a domain of about 537 to 554 nm. (Brown, 2019)

their sum, the total angular momentum J. Our description above of the transition $^3S_1 \rightarrow {}^3P_2$ uses the standard notation for their quantum properties. In particular, ${}^{2S+1}[L]_J$ where the angular momentum L is quantized by $[S] = L = 0$ and $[P] = L = 1$.

When there is no magnetic field applied, the change in orbital increases the total angular momentum J from 1 to 2. With a magnetic field applied, however, this transition splits into multiple possible transitions. These are intrinsically related to the initial and final angular momentum numbers in J; as in the subdivided line m_J corresponds thusly:

$$J = 1 \rightarrow m_J = \pm 1, 0$$

$$J = 2 \rightarrow m_J = \pm 2, \pm 1, 0$$

So, we can see that the initial state is subdivided into three possible states while the final state is subdivided into five possible states.

Under the rules of quantum mechanics, however, the maximum transition magnitude is |1| such that $\Delta m_J = \pm 1, 0$. Moreover, these transitions occur linearly polarized, in directions perpendicular to one another. The set which we dub π corresponds to $\Delta m_J = 0$ in which emission is polarized along the direction of the magnetic field (horizontally with respect to our optical rail). Conversely, the set σ corresponds to $\Delta m_J = \pm 1$ in which the emission is polarized perpendicular to the magnetic field (and vertically to our optical rail). Figures Three (a) and (b) illustrate these transitions and their relative intensities to one another.

The energy of the emission is proportional to the number m_J, wherein $\delta E = g\mu_0 B m_J$ (Brown, 2019).

Figure Two: The Fabry-Perot Interferometer

(a) The mirrors of the Fabry-Perot

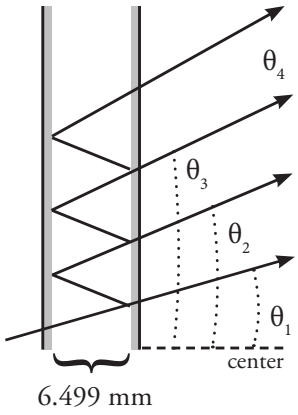

(b) Interference pattern (B=0)

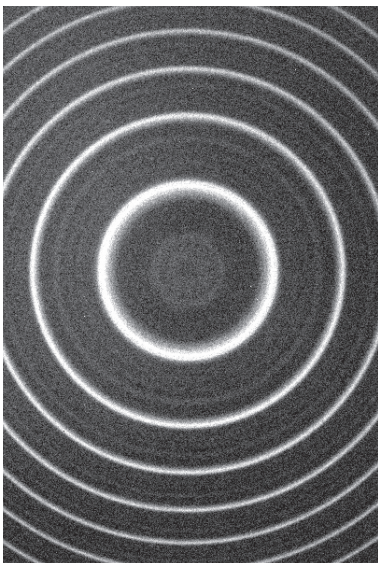

The Fabry-Perot interferometer is unique in that its total path length for each order is proportional the number of reflections made within the spectrometer. Each subsequent reflection produces another fringe at a different angle; accumulation results in regularly spaced circular fringes spaced like that of (b). Note that this image of the fringes are with the electromagnet turned off (B=0). (Brown, 2019)

Figure Three: Transitions in Mercury $^3S_1 \rightarrow {}^3P_2$ with a magnetic field applied

(a) π polarization: $\Delta m_J = 0$

(b) σ polarization: $\Delta m_J = \pm 1$

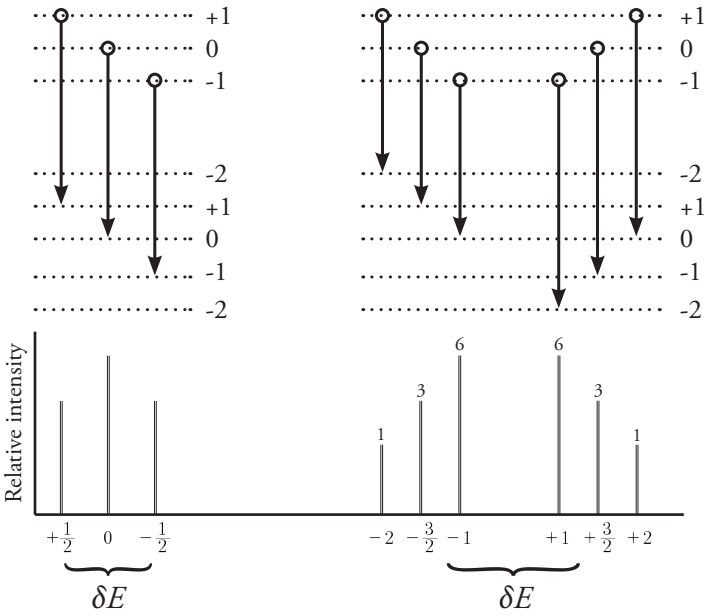

Each of the π and σ polarizations correspond to a different change in the quantum number m_J. If this number does not change -- as in $\Delta m_J = 0$ -- the π polarization occurs parallel to the magnetic field. The perpendicular σ polarization is true for $\Delta m_J = \pm 1$.

These transitions have differing intensities relative to one another, and the separation between their peaks can be quantified as δE, used to calculate the Bohr magneton.

The unitless constant g is quantified by $g = 1 + \frac{J(J+1) + S(S+1) - L(L+1)}{2J(J+1)}$, wherein the variables J, S and L are those quantum numbers associated with the initial and final states. The initial state has a value $g = 1 + \frac{2+2-0}{2\times 2} = 2$ whereas the final state has a value $g = 1 + \frac{6+2-2}{2\times 2\times 3} = \frac{3}{2}$.

The Bohr magneton μ_0 is a physical constant of the universe. It represents the magnetic moment of the electron, which includes its orbital and spin momenta; and thusly it can be represented as $\mu_0 = \frac{e\hbar}{2m_e c}$ involving the fundamental charge *e*, the Planck constant $\hbar$, the mass of the electron m_e and the speed of light *c*. These values are require understanding of quantum mechanics which hadn't been developed in Zeeman's time. In collaboration with Lorentz, however, the derivation of this constant stands as the first quantification of the properties of the electron (Brown, 2019).

In order to apply a magnetic field and polarize the resultant light, we need to add two more elements to the optical rail. The first is, of course, the electromagnet with an attached Hall probe to measure the correspondent magnetic field. The second is a polarizing lens, which can be changed to 0° or 90° polarizations. The entire assembly is depicted in Figure Four.

The goals of this lab report are twofold.

First, I will verify the relationship between the angle θ and wavelength and the spacing of the Fabry-Perot interferometer. We will calculate at zero magnetic field strength the slope of θ^2 to confirm that $\frac{d\theta^2}{dt} = \frac{\lambda}{t}$.

Second, for each the π and σ polarizations, I will calculate the Bohr magneton from the energy spacings between the interference lines, as shown in Figure Three.

This paper will reference these values to accepted theoretical values and produce a p-value to reflect the certainty in our results.

This report is organized in the following sections, including relevant data and bibliographical information placed in the Appendix:

Figure Four: Full diagram of the Optical Rail

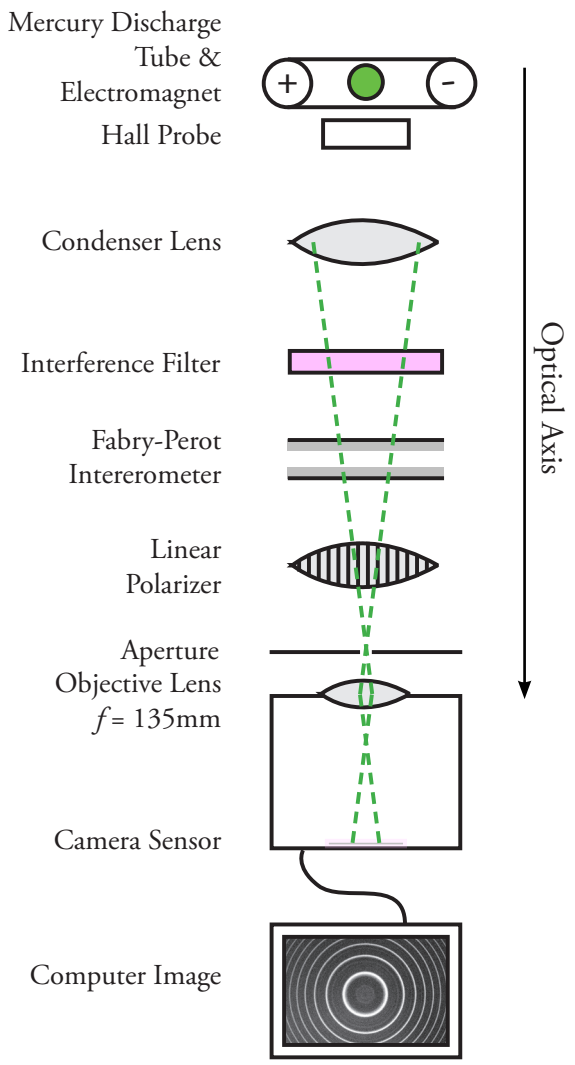

Starting from the top, this diagram illustrates the light path as it passes through each of the optical components on the rail. The discharge tube emits multiple wavelengths from transitions in Mercury's orbitals, multiplied further by the influence of an electromagnet through the Zeeman effect. This light is condensed and passed through an interference filter, eliminating all but a specific desired band of wavelengths around 546 nm. A Fabry-Perot interferometer repeatedly reflects light and creates interference fringes like those described in Figure Two. The linear polarizer polarizes light either 0° or 90° to the optical rail. Lastly, an aperture blocks out all but the center of the light and an objective lens focuses this onto the camera sensor, which is assembled by the computer into an image.

This image can then be processed into a horizontal profile, which highlights the peaks and troughs of the image, producing a dataset like that in Figure Five.

Methods & Procedures

Perhaps the first important point is to describe the conversion of an image into its correspondent horizontal profile like that of Figure Five. As we see, the relative intensity of the light is described as a correspondent value on the vertical axis of the profile. There is also a level of ambient noise, as displayed in (b) which systematically offsets the data. We can quantify this noise with a horizontal profile set and subtract it from the dataset, which we demonstrate in (c).

The horizontal profile describes the position of this intensity from 0 to 765, which covers the horizontal pixel count of the image. To ease the process of data analysis, this will be how our fringes will be counted.

As the horizontal axis is not centered, we need to compute a central point from which to consider our angles θ. We can average the distances between each of the primary peaks of Figure Five (when B = 0) and find a number with an associated standard deviation which we can apply in our further error propagation.

The calculation of θ is described by the rather simple geometries associated with the Fabry-Perot and the objective lens. Referencing both Figures Two and Four, we can determine that $f\theta = (9\,\mu m) \times n$ where n is our number of pixels multiplied by the resolution of 9 μm and f is the focal length of the camera objective lens, 135mm.

We can solve this equation for θ to find the angle for any pixel from the center.

Verification of $\frac{d\theta^2}{dt} = \frac{\lambda}{t}$

The first in our list of goals is the relationship between the slope of θ^2 and the wavelength of light and Fabry-Perot separation.

We perform this analysis on the fringes produced by the optical rail when the electromagnet is turned off (that is, B = 0). Regardless of the polarization (π or σ), the interference fringes produced will be the same if there is no magnetic field influencing the emissions. In our case, we use two images to calculate both a zeropoint to center our data and, subsequently, the calculations for θ deviation from the center.

Squaring this value, and finding the slope using the method of least squares, we find a slope $\frac{d\theta^2}{dt}$ for each of the images.

Comparing the value we receive calculating $\frac{\lambda}{t}$, we can determine the level of agreement between them.

Figure Five: The process of obtaining a horizontal profile, subtracting noise from the data

(a) Image of Interference pattern with electromagnet off

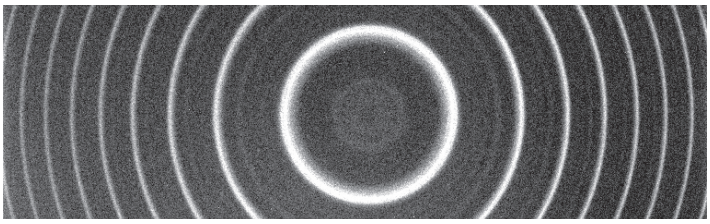

(b) Ambient noise with discharge tube off

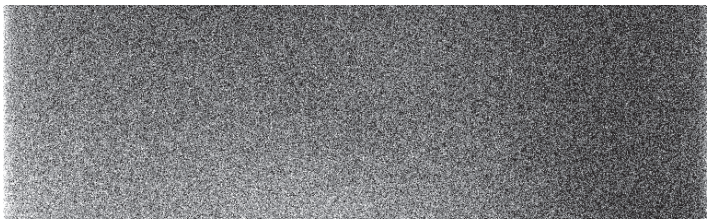

(c) Horizontal profile of (a) with noise from (b) subtracted

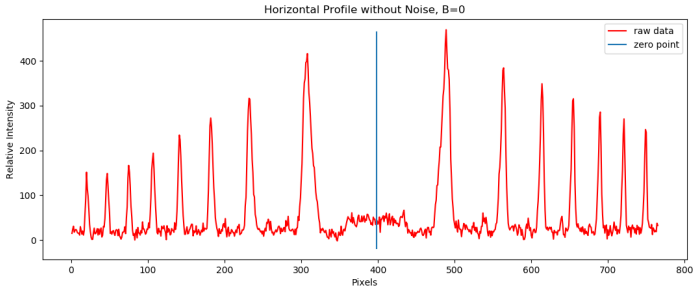

Having obtained an image for our interference pattern, we can then take another set of data for the background noise. In our case, we took four images of the background noise to find an average error under multiple conditions. We decided not to propagate error from it as the standard deviation was very low.

Taking the horizontal profiles of each, we can find our corrected profile for the interference fringes (a) by subtracting the average noise (b) from the set. The resulting corrected image is shown in (c).

With this data, we can accurately determine the peaks' spacing from the zero-point, highlighted as the blue line, and determine the respective angle θ using our equation described in the beginning of this section.

Analysis of π polarized interference fringes

Starting with 0° polarization, let's investigate how the horizontal profile appears, and how we go about solving for δE which we will need to calculate the Bohr magneton.

Each horizontal profile like that of Figure Six (a), has a correspondent magnetic field strength it is associated with. As we know, the magnetic field increases an energy gap which is proportional with the field strength. Therefore, as we increase in B, we expect the gap δE to increase proportionally.

In the case of π polarization, we know the lower-intensity $m_J = \pm 1$ lines occur evenly spaced from higher-intensity $m_J = 0$ lines, as shown in Figure Three (a). The experimental data in Figure Six demonstrates this exactly, with a single dominant peak saddling two smaller peaks.

Leveraging the equation relating θ_a and θ_b correspond to their wavelengths and difference in energy, $(\theta_p^{(a)})^2 - (\theta_p^{(b)})^2 = 2\overline{\lambda}(\frac{1}{\lambda_a} - \frac{1}{\lambda_b}) = 2\frac{E_a - E_b}{\overline{E}}$ (Brown, 2019), we can reference Figure Six (b). We can use the spacing between the two sub-peaks we can define $E_a - E_b = \Delta E = (\frac{1}{2}\delta E)$ such that

$$\Delta\theta_{ab}^2 = 2\frac{\Delta E}{\overline{E}} = 2\frac{(\frac{1}{2}\delta E)}{\overline{E}}$$

$$\Delta\theta_{ab}^2 \times \overline{E} = \delta E$$

$$\Delta\theta_{ab}^2 \times \overline{E} = 2\mu_0 B m_J \quad where \;\; m_J = +1$$

$$\mu_0 = \frac{\Delta\theta_{ab}^2 \times \overline{E}}{2B}$$

specifically for the π polarization.

The average energy $\overline{E} = \frac{\hbar c}{\overline{\lambda}}$ correspondent to our known value for the average wavelength.

For each set of peaks we can discern Figure Six (a), we can perform this analysis to solve for the value of the Bohr magneton. As the magnetic field increases, however, the energy spacing will continue to increase, eventually such that the peaks begin to overlap with others and noise takes over. Additionally, there exists a general level of noise which takes over the profile as a whole. For this reason, our measurements of this polarization are bounded by (500 < B < 1100) milliTesla and about ten peaks per profile (five per side).

Figure Six: Obtaining δE from π polarized profiles

(a) Horizontal profile of the Zeeman effect at B = 657.3mT

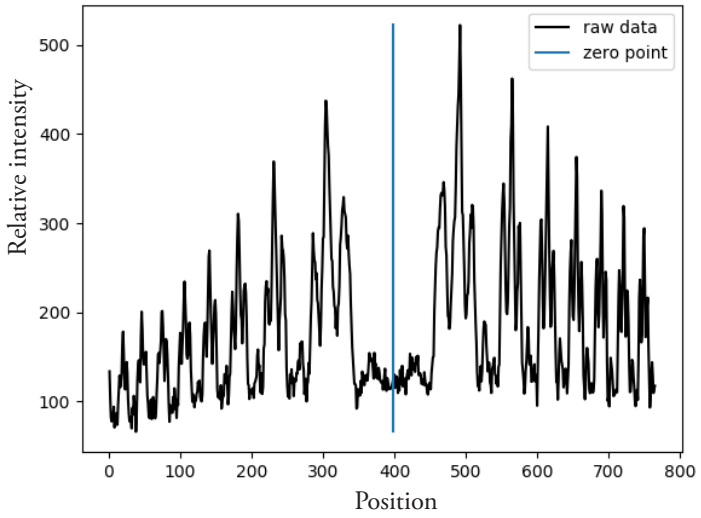

(b) Close-up of energy separations at angles θ

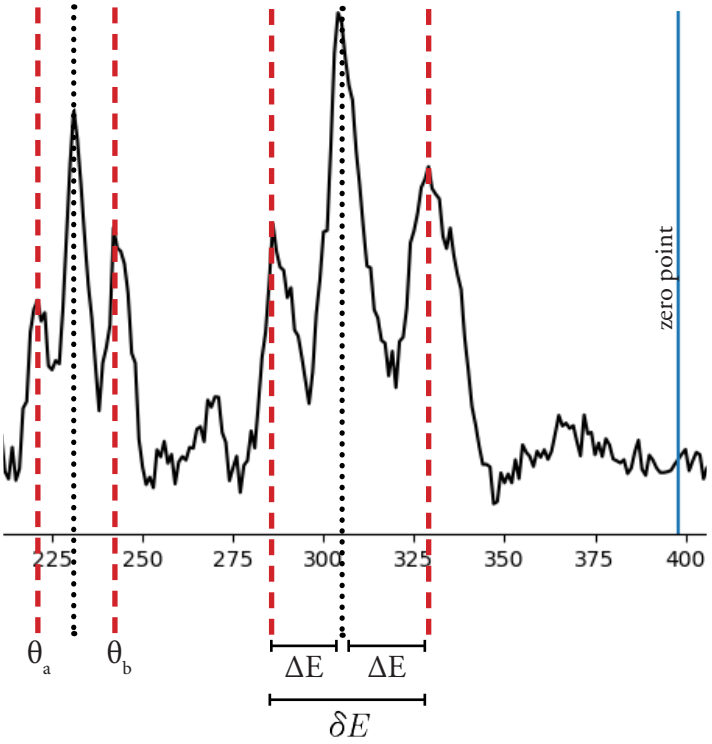

This example profile is at a magnetic field strength 657.3mT, with about six discernible peaks per side. Zooming into a couple peaks, we can easily see the difference in relative intensity and the equally spaced energy gaps between the major- and sub-peaks.

These energy gaps we define as ΔE which are related to the Bohr magneton by the mathematics defined to the left. Specific to this diagram, we can see that the term $2\mu_0 B m_J$ is defined by m_J, which itself is clearly transitions to 0 and ±1, with the major peak as the former and the subpeaks as the latter.

Analysis of σ polarized interference fringes

Turning our polarizer to 90°, we get a profile similar to that of Figure Seven (a). Similar to the π polarization, the spacing between the peak sets increases proportionally to the magnetic field strength.

In the case of σ polarization, however, the two minature peaks actually correspond to six different transitions which correspond to final values of $m_J = \pm 2, \pm 1$ and 0. These transitions have relative intensities and positions shown in Figure Three (b), however the profile in Figure Seven clearly shows just two peaks per set. This is because our camera resolution is too low to pick up all three distinct lines.

In order to accurately measure these lines, we need to find the weighted average of the position of these lines based on their intensity. Using a simple method of finding the arithmetic mean, we get a separation $\sim m_J = 5/4 = 1.25$. When we measure the individual angles and utilize them in our equations, we include this in the place of our value m_J.

Starting in the same place as we did for π polarization, we can find the we can use the spacing between two peaks as $E_a - E_b = \Delta E = \delta E$ such that

$$\Delta\theta_{ab}^2 = 2\frac{\Delta E}{\overline{E}} = 2\frac{(\delta E)}{\overline{E}}$$

$$\Delta\theta_{ab}^2 \times \overline{E} = 2(\delta E)$$

$$\Delta\theta_{ab}^2 \times \overline{E} = 2\left(\frac{3}{2}\mu_0 B m_J\right) \quad where\ m_J = +\frac{5}{4}$$

$$\mu_0 = \frac{\Delta\theta_{ab}^2 \times \overline{E}}{\left(\frac{15}{4}\right)B}$$

specifically for the σ polarization.

Similar to our other polarization, there are bounds where noise overtakes these relatively low-intensity peaks or the magnetic field separates them too far. In the case of σ polarization, our set ranges from (125 < B < 500) milliTesla and about ten peaks per profile.

Figure Seven: Obtaining δE from σ polarized profiles

(a) Horizontal profile of the Zeeman effect at B = 128.6mT

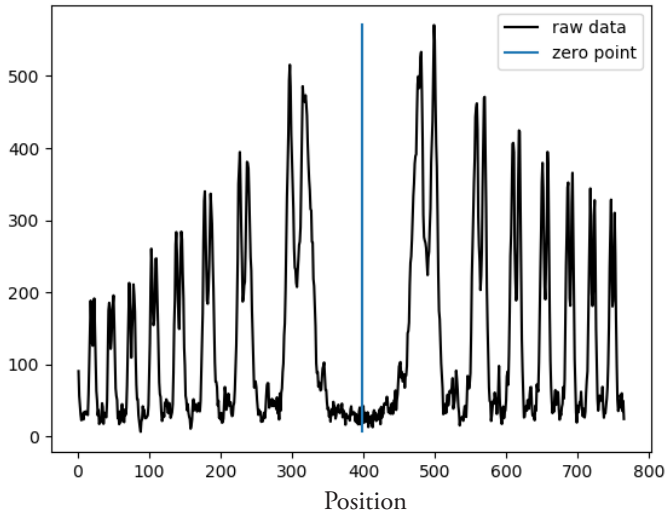

(b) Close-up of energy separations at angles θ

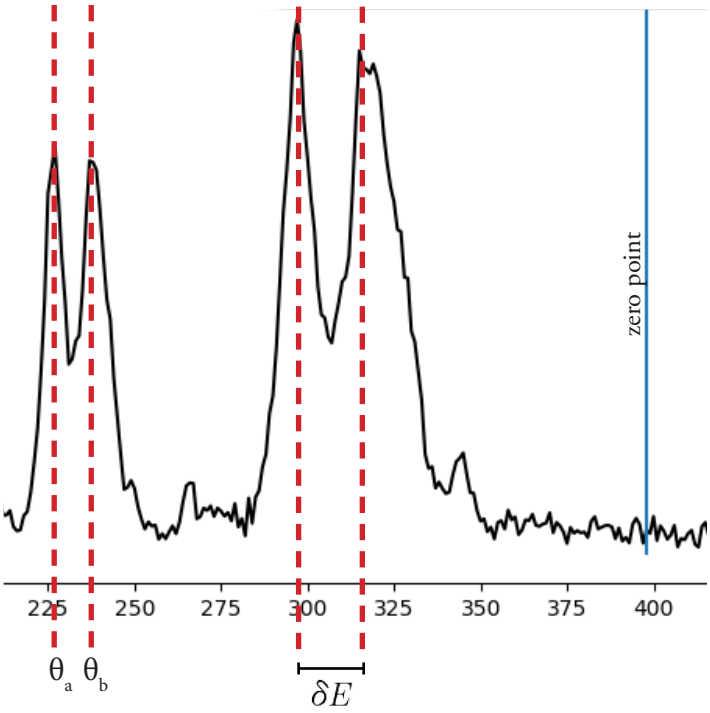

In this example, the magnetic field strength is 128.6 mT. (b) demonstrates the spacing of the lines, which are evaluated downstream as a weighted average of three transmission lines per peak described in Figure Three (b). These peaks are too small for the resolution of our camera. Importantly, it means that the equation for the calculation of the Bohr magneton involves a quantum momentum number $\sim m_J = 1.25$ as the weighted average for the indiscernible peaks.

Error Analysis

Some discussion must specifically be had over the choice of error, its propagation, and our standards for determining whether our measurement is in good agreement with theory.

Firstly, with the calculated zero point, we determine our error in the measurement of pixel position based on the variance σ^2 from this calculation. We determine the error to be the square root of the set's variance, or its standard deviation. Say some value q has a variance σ_q^2 -- its error will be $\sigma_q = \delta q$. We can represent this value as $q_i \pm \delta q_i$.

There are various different external values which we attach error in order to accurately represent the role of their variation at such small scales. For the average wavelength λ and mirror separation t, for example, we attach a deviation of 0.5 to the finest order we are given. For λ = 597.3 nm we attach ±0.05 nm to compensate for any variance therein. In the case of $\frac{\lambda}{t}$, we come to a unitless value of $(8.402 \pm 0.769) \times 10^{-5}$ with which to compare to our experimental value.

Values which are universal and independent from the materials we are given, specifically the Bohr magneton, use previous studies to determine their value and error in this report. Our value for the magneton is thusly $\mu_0 = 9.2740100783 \times 10^{-24} \pm 2.8 \times 10^{-33}$ J/T (CODATA, 2018).

When propagating error, we will use the rule of quadrature. For some function $q(x_1,x_2,...,x_n)$ with associated errors δx_i, the error for that function is:

$$\delta q = \sqrt{\sum_i^n \left(\frac{dq}{dx_i}\delta x_i\right)^2} = \sqrt{\left(\frac{dq}{dx_1}\delta x_1\right)^2 + \ldots + \left(\frac{dq}{dx_n}\delta x_n\right)^2}$$

This propagation occurs for any arithmetic operations that contain values with an attached uncertainty. The average energy $\overline{E} = \frac{\hbar c}{\overline{\lambda}}$, for example, has error available to be propagated from λ such that the value $\overline{E} = (3.617 \pm 0.0003) \times 10^{-19}$ J.

For each equation, we repeat this process so that we arrive on a final value and weight for each value which we want to compare.

Figure Eight: The Gaussian Distribution

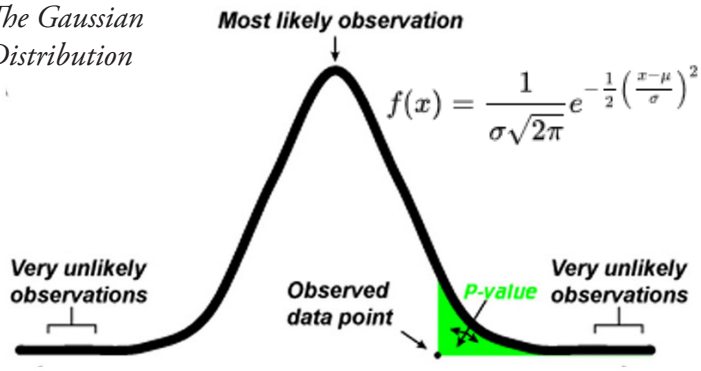

The Gaussian Distribution takes in our combined uncertainty to produce a distribution which evaluates the probabilistically 'best' value. With this, we can calculate the area under the curve from our data point (which will be the deviation from the accepted value) and find a p-value. This value informs our evaluation of the accuracy of experimental results.

Reaching the final value and uncertainty may involve the averaging of numbers with respect to their weight. This process, where we find the weighted average of a set, is defined by the following equation:

$$x_{avg} \pm \delta x_{avg} = \frac{\sum_0^i w_i x_i}{\sum_0^i w_i} \pm \frac{1}{\sqrt{\sum_0^i w_i}}$$

The weight σ for our Gaussian Distribution will then be the error propagated from the experimental and reference values for an uncertainty about the mean of the values.

Looking at Figure Eight, we see the equation for the Gaussian distribution, which defines its own error parameter σ and a center for the function, μ. We want to center our distribution at x = 0 for simplicity's sake, so we choose μ = 0.

The coefficient of the Gaussian Distribution normalizes the distribution, such that the integral over its full bounds (-∞,∞) resolves to one. For this reason, the p-value suggests a percent likelihood that a given value is correctly obtained.

Results

The first piece of information we need to establish is the calculation of a zero-point. Using both datasets, we use the methods described in the prior section and recieve a value for the center z = 398.14 ± 0.23 pixels. As we do not move the camera or change any of its settings throughout the 2-hour data collection period, we can assume that the zero point is identical for each of the images throughout this experiment.

Verification of $\frac{d\theta^2}{dt} = \frac{\lambda}{t}$

Our first goal is to plot the values we obtain for θ^2 against their correspondent order. We took two datasets when the magnetic field strength was zero, so it makes sense to calculate two sets of this data for higher precision. While these plots are separated in Figures Nine (a) and (b), it needs specific emphasis that the polarization lens does not affect the data when the magnetic field is negligible. This is to say that both images where B = 0 are theoretically identical.

Regardless, we can take the least square regression of each left- and right-side order slopes of θ^2 and compare them to the theoretical value which is colored blue for each plot in Figure Nine. As we can clearly see in (a) and (b), there is a visually high level of correlation between the values.

Propagating error and taking the slopes and plotting the experimental $\frac{d\theta^2}{dt}$ and theoretical $\frac{\lambda}{t}$ in (c), we see that the values are rather close. The error in the theoretical value far outpaces that of the experimental error, however, with the former having an error of roughly 7.69×10^{-6} degrees^2 and the latter on the order of 10^{-10}. This is largely because the standard deviation in the measurement of the zero point is small enough that the error is reduced significantly when propagated by the rule of quadrature ($0.22 \times 9 \times 10^{-6}$). For now, proceed with further explanation to come in the *Discussion* section.

Taking these respective uncertainties and following our guidelines for error analysis, we take the weighted average of the values from the π and σ polarizations which comes to $\frac{d\theta^2}{dt}$ = 8.505 with a negligible error on the order of 10^{-10}.

Creating the Gaussian distribution shown in Figure Ten we get a one-tailed p-value of 0.447. This suggests strong agreement, however one must note that the relatively high error in the theoretical value drives the particularly strong correlation.

Figure Nine: Analysis of θ^2 versus Order with B = 0

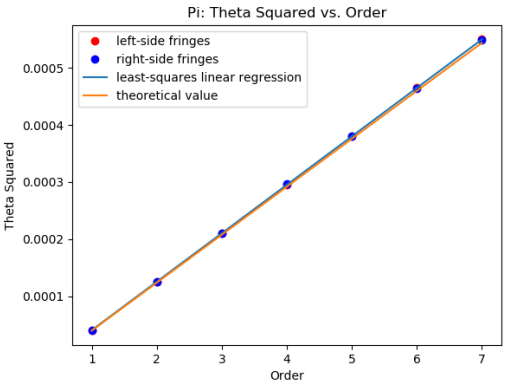

(a) Comparison of θ^2 versus Order for π polarization

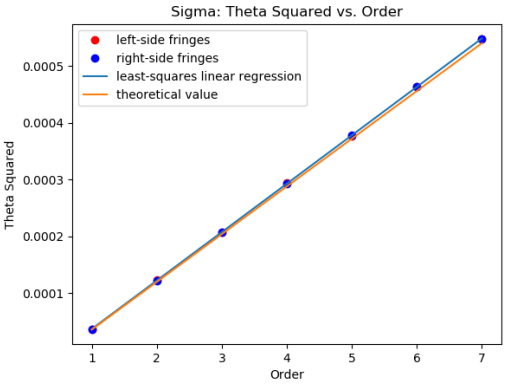

(b) Comparison of θ^2 versus Order for σ polarization

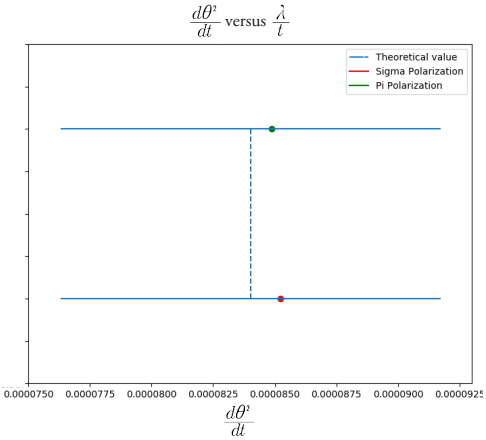

(c) Theoretical $\frac{d\theta^2}{dt}$ with error plotted against calculated value for π and σ

The first, most important point to note is that with a negligible B field strength, there actually is no difference between π and σ polarizations. In fact, their values should be practically equal. There is, of course, some variation which occurs on a minute order.

The first two figures track the two polarizations' left- and right-order θ calculations for each order. As we discuss, their linear slopes are correspondent with the theoretical value (orange) $\frac{\lambda}{t}$.

Taking a least-squares linear regression of their combined data (blue) we can compare those calculated slopes from each set to the theoretical value in (c). Error in both the theoretical and experimental data is propagated, however the error for the experimental sets is on a miniscule order (10^{-10}) and so does not even appear compared to that of the theoretical. This is acceptable due to the high correlation and is elaborated upon further in the *Discussion* section.

The resulting data is fed into our analysis of error and we get a resultant p-value of 44.7%.

Figure Ten: Gaussian Distribution of the theoretical versus reference value for $\frac{\lambda}{t}$

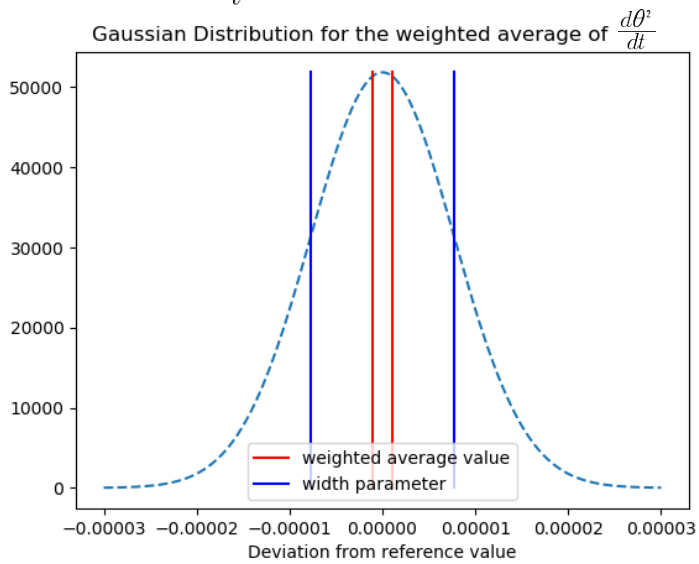

This Gaussian distribution combines the uncertainties attached to the reference value $\frac{\lambda}{t}$ with the error in our weighted average of $\frac{d\theta'}{dt}$ to create a probability distribution for the likelihood of our value being collected. In this case, the one-tailed p-value is found to be 44.7%, indicating good agreement.

Derivation of the Bohr magneton from π polarized interference fringes

From a selection of six clean datasets in varying magnetic field strengths, we produce a set of values for the Bohr magneton shown in Figure Eleven (a). The magnetic field strength varies from 512.2 to 1,092 mT, which are shown in Figure Eleven (b) to demonstrate the appearences of these fringes at their extremes. Specifically, this figure includes the computed 'corners' of the dataset, highlighting the maxima and minima in red and green dots respectively.

We combine all of these values in a weighted average to create our Gaussian Distribution in Figure Eleven (c) for the Bohr magneton at π polarization to get a value of $\mu_0 = (9.662 \pm 0.135) \times 10^{-24}$ J/T.

This value results in a one-tailed p-value of 0.130, or a likelihood of having performed the experiment correctly and gotten this result of 13%.

This value indicates agreement, meaning that our experimental process and mathematics are were likely performed accurate to reference value we are comparing against.

Figure Eleven: Analysis of the Bohr Magneton using π polarized interference fringes

(a) Comparison of derived values of the Bohr magneton to the weighted average and reference values

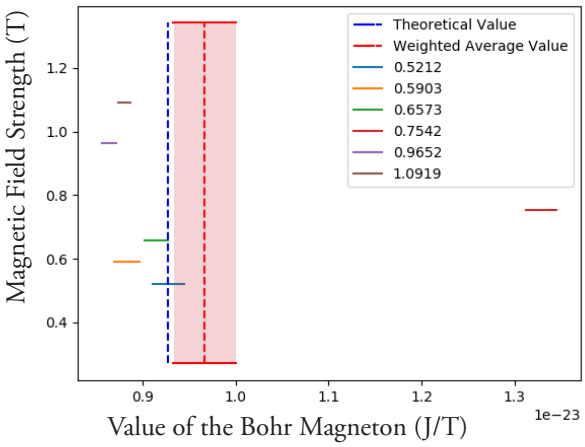

Each bar represents a value with attached error.

The shaded red represents the weighted average error.

(b) Horizontal profiles of the lowest and highest magnetic field strengths calculated

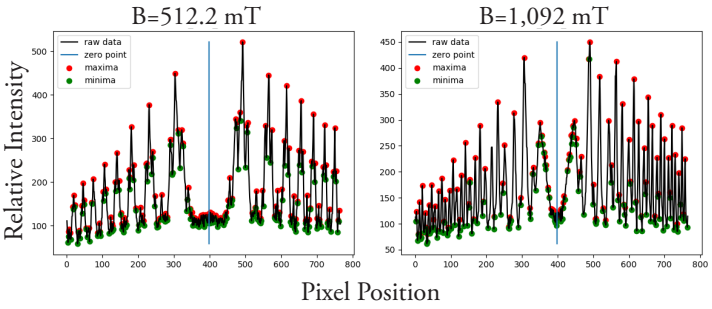

(c) Gaussian Distribution comparing the weighted average and reference values of the Bohr magneton

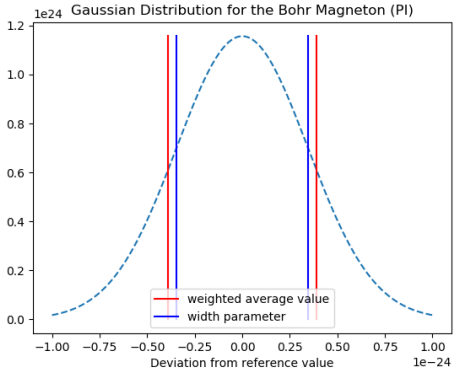

The first figure, (a), compares the calculated Bohr magnetons for each π polarized set against one another. Ordered by their magnetic field strength, they have a line which demonstrates their associated error and includes the weighted average value (error in light red) and the reference value.

These values varied in separation due to the variation in magnetic field strength demonstrated in (b). The magneton values in (a) and their correspondent errors are propagated with the error in the reference value and used to create the Gaussian probability distribution seen in (c).

This distribution reveals a one-tailed p-value of 13%, indicating good agreement.

Derivation of the Bohr magneton from σ polarized interference fringes

Similar to the last, we take a series of five datasets of varying field strengths from 128.6 to 448.1 mT. The lower range of magnetic fields reflects the larger separation that the states produce which means that they more easily overlap by the time field strengths reach 600-or-so mT. We calculate the correspondent set of Bohr mageneton values and show them in Figure Twelve (a). Figure Twelve (b) shows the horizontal profiles at the maximum and minimum field strength values including the maxima and minima for highlighted for each respectively.

We combine all of these values in a weighted average to create our Gaussian Distribution in Figure Twelve (c) for the Bohr magneton at σ polarization to get a value of $\mu_0 = (8.673 \pm 0.369) \times 10^{-24}$ J/T.

This value results in a one-tailed p-value of 0.254, or a likelihood of having performed the experiment correctly and gotten this result of 25.4%.

While this value is numerically further to our reference value compared to the value we had for π polarization, the uncertainty attached to the σ calculation increases the width of the Gaussian and therefore brings the weighted average within fewer standard deviations of the mean.

As such, this value indicates agreement, meaning that both calculations for the Bohr magneton are in good agreement with theory and suggests that our experiment has a good probability of being accurate.

Discussion

The remainder of this report is dedicated to the discussion of the results, how they reflect our methodology and additional recommendations and improvements for future experimentation.

Firstly, addressing the experimental calculation of $\frac{\lambda}{t}$, it is important to note that while the propagation of error for the theoretical value was correctly done, the experiment would be improved with a more rigorous measurement of the average wavelength to perhaps a few more decimals. Frankly, the low variation in the zero-point and the high correlation for the experimental data minimized the error drastically in the mathematics. As such, the theoretical error dominated the Gaussian width and resulted in a comfortable agreement.

In most cases, we would expect a lower p-value and the fact that our value is so high suggests a need

Figure Twelve: Analysis of the Bohr Magneton using σ polarized interference fringes

(a) Comparison of derived values of the Bohr magneton to the weighted average and reference values

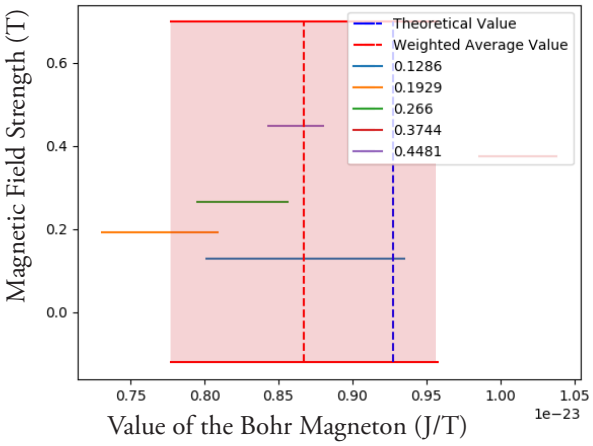

Each bar represents a value with attached error.

The shaded red represents the weighted average error.

(b) Horizontal profiles of the lowest and highest magnetic field strengths calculated

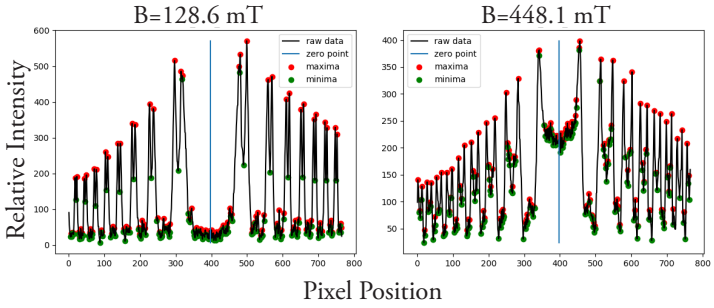

(c) Gaussian Distribution comparing the weighted average and reference values of the Bohr magneton

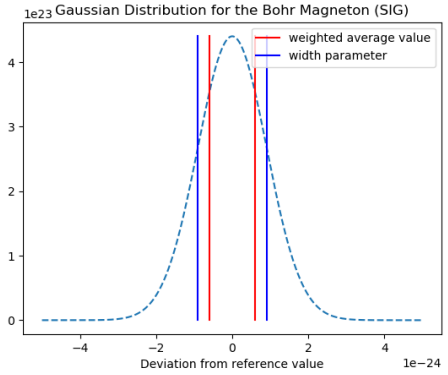

The magneton values for σ polarization are calculated and compared against one another, the weighted average value and the reference value in (a).

They are ordered by their magnetic field strength, which proportionally varies the energy separation; the extremes of which are demonstrated by (b). Here, the lowest and highest magnetic field strengths and their resultant energy separation are shown.

Lastly, (c) propagates the error in the weighted average value and the reference value to create a Gaussian probability distribution with a one-tailed p-value of 25.4%, indicating good agreement.

for concern. I found no mathematical errors in the few operations it takes to calculate the uncertainty, which suggests that the reference value simply requires a finer precision to be tested best. For our purposes, however, the correlation stands and we can experimentally verify this principle.

For both the π and σ polarizations, there is quite a bit of variation between calculated values of the Bohr magneton. The resultant weighted average values, however, hover around a similar area and, as such, reflect that though the resolution of the camera is low, the number of trials and data points collected is able to reduce random noise in our measurements.

Specifically, there is no evident systematic error. The values don't follow any pattern regarding their magnetic field strength and they are largely within three standard deviations of the reference value with the exception of B = 754.2 mT in the π polarization group.

As such, there is little reason to believe that the generally good p-values of 0.13 and 0.254 for the π and σ polarizations, respectively, have any inherent problems. Future experiments could increase the size of the dataset and the number of points collected to become increasingly precise and drown out the noise from the camera sensor. They could additionally invest in a higher resolution camera and a more precise Hall probe.

That being said, however, the values obtained in this report are largely in good agreement with little more to recommend in terms of precision than more data and better equipment.

At a higher level, these results are evidence of two important points. First, that the Zeeman effect is intrinsically linked to the quantum-mechanical properties of the electron and its angular and orbital momentum. Second, that Zeeman and Lorentz truly did discover properties of the electron before the particle was experimentally discovered.

The experimental analysis of the Zeeman effect kicked off a field of study which culiminated in a deep understanding of the structure of the atom, the subatomic particles within it and the quantum interactions that they produce. More than a century later, that research continues in the Standard Model, with new and different exotic particles and force-carries being produced, parsed out and published in linear accelerators around the world. Zeeman's effect on the history of the electron is perhaps more difficult to quantify than the natural phenomena named after him.

Appendix

Bibliography

Zeeman, Pieter (February, 1897). The Effect of Magnetisation on the Nature of Light Emitted by a Substance. Nature Vol. 55. (Accessed March 14, 2020). Retrieved from https://hdl.handle.net/2027/mdp.39015024088695?urlappend=%3Bseq=238.

Brown, George. Physics 134 Advanced Laboratory Manual: The Zeeman Experiment (p.123 - 131) & Appendix: The Fabry-Perot Interferometer (p. 132 - 136)

2018 CODATA recommended values (May 20, 2019). Bohr Magneton. National Institute of Science and Technology. (Accessed March 14, 2020). Retrieved from https://www.physics.nist.gov/cgi-bin/cuu/Value?mub